Cosmogenic radiosulfur tracking of solar activity and the strong and long-lasting El Niño events

Mang Lin[a,b,c,d,1] and Mark H. Thiemens[e]

Edited by Akkihebbal Ravishankara, Colorado State University, Fort Collins, CO; received November 29, 2021; accepted March 29, 2022

Reconstruction of past solar activity or high-energy events of our space environment using cosmogenic radionuclides allows evaluation of their intensities, frequencies, and potential damages to humans in near space, modern satellite technologies, and ecosystems. This approach is limited by our understanding of cosmogenic radionuclide production, transformation, and transport in the atmosphere. Cosmogenic radiosulfur (^{35}S) provides additional insights due to its ideal half-life (87.4 d), extensively studied atmospheric chemistry (gas and solid), and ubiquitous nature. Here, we report multiyear measurements of atmospheric ^{35}S and show the sensitivity of ^{35}S in tracking solar activity in Solar Cycle 24 and regional atmospheric circulation changes during the 2015/2016 El Niño. Incorporating ^{35}S into a universal cosmogenic radionuclide model as an independent parameter facilitates better modeling of production and transport of other long-lived radionuclides with different atmospheric chemistries used for reconstructing past astronomical, geomagnetic, and climatic events.

solar cycle | ENSO | cosmic rays | cosmogenic radionuclides | sulfur-35

As the primary energy source of the solar system, the Sun controls the Earth's climate and hydrological system and surface radiative energy budget and is crucial in sustaining life and Earth's habitability (1–5). The solar forcing of changes in Earth's atmosphere (from the exosphere to surface) is an active area of research in Earth and space sciences. Cosmogenic radionuclides, created by the interaction of high-energy galactic cosmic rays (GCRs) and atoms/molecules in Earth's atmosphere (e.g., O_2, N_2, and Ar), embed in atmospheric circulation and incorporate into the hydrosphere, cryosphere, biosphere, pedosphere, and lithosphere following deposition on Earth's surface. Solar activity plays a crucial role in controlling cosmogenic radionuclide abundance by modulating the flux of GCRs around Earth and protects Earth from GCRs penetrating its geomagnetic field (Fig. 1*A*). Relatively long-lived cosmogenic radionuclides (e.g., ^{14}C and ^{10}Be) in geochemical proxies such as tree rings and ice cores are utilized to reconstruct past solar activity and geomagnetic field strength (1–6). Yearly resolved anomalies were attributed to strengthened GCRs modulated by abrupt declines in solar activity or increased fluxes of accelerated high-energy atomic nuclei from high-energy astronomical events such as solar proton events (SPEs) and supernovae (SNe) (2, 4), which may potentially lead to mass extinction events (7).

Cosmogenic radionuclide anomalies are expected to be observed globally. Spatial variabilities potentially due to chronology problems were recently reported, leading to active debates on sources of cosmogenic radionuclide anomalies (5). Such spatial variability, especially in aerosol-bound radionuclides (e.g., ^{10}Be), is also controlled by climate-induced regional atmospheric circulation changes (2, 6). Therefore, a global cosmogenic radionuclide model that precisely describes production, transformation, and transport of all cosmogenic radionuclides at high spatial–temporal resolution is required to separate astronomical, climatic, and geomagnetic components in cosmogenic radionuclide records (2, 6, 8, 9). Measurements in the modern atmosphere are important for developing this model. The short atmospheric residence time of aerosols relative to $^{14}CO_2$ is important for tracking solar activity (2, 3), and measurements of aerosol-bound cosmogenic radionuclides such as ^{7}Be and ^{10}Be have been widely utilized (6, 8). Modeling their transport in the atmosphere is, however, challenging because it is inadequately understood how these radionuclides preferentially attach to chemical complex aerosol components such as sulfates (6). Radiosulfur (^{35}S) (half-life: 87.4 d) may provide additional and more ideal constraints because sulfur chemistry and transport are extensively studied and simulated in atmospheric chemistry transport models given their roles in acid rain, public health, and climate changes. Radiosulfur is predominately produced in the stratosphere via spallation of Ar by GCRs (10) and participates in the Earth's sulfur cycle via the rapid (∼1 s) oxidation to radiosulfur dioxide

Author affiliations: [a]State Key Laboratory of Isotope Geochemistry, Guangzhou Institute of Geochemistry, Chinese Academy of Sciences, Guangzhou 510640, China; [b]CAS Center for Excellence in Deep Earth Science, Guangzhou Institute of Geochemistry, Chinese Academy of Sciences, Guangzhou 510640, China; [c]Southern Marine Science and Engineering Guangdong Laboratory (Guangzhou), Guangzhou 511458, China; [d]University of Chinese Academy of Sciences, Beijing 100039, China; and [e]Department of Chemistry and Biochemistry, University of California San Diego, La Jolla, CA 92093

Author contributions: M.L. and M.H.T. designed research; M.L. performed research; M.L. and M.H.T. contributed new reagents/analytic tools; M.L. analyzed data; and M.L. wrote the paper.

The authors declare no competing interest.

[1]To whom correspondence may be addressed. Email: linm@gig.ac.cn.

This article contains supporting information online at http://www.pnas.org/lookup/suppl/doi:10.1073/pnas.2121550119/-/DCSupplemental.

Published May 6, 2022.

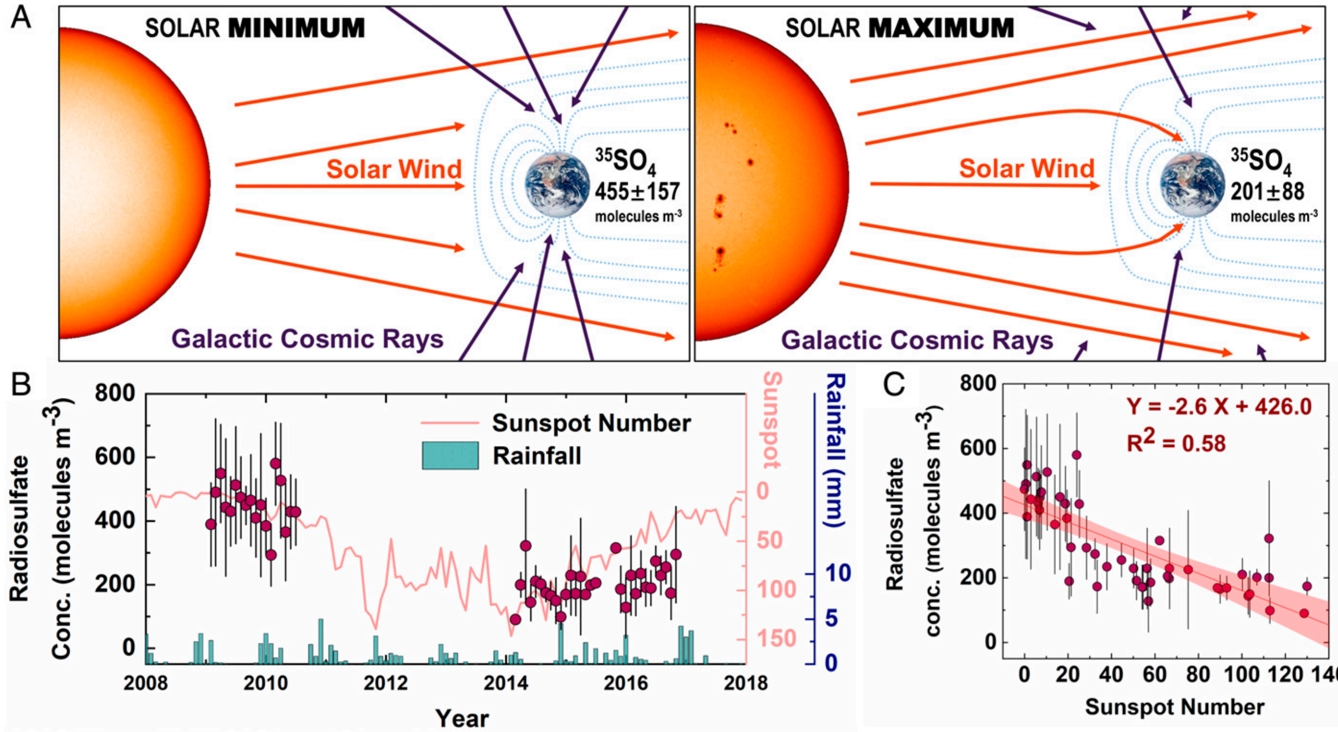

Fig. 1. (*A*) Schematic graphs showing how the strength of solar activity (characterized by sunspot numbers) influences atmospheric ^{35}S concentrations. In solar minimum, weaker solar wind allows less modulation and more high-energy cosmic rays get through, leading to higher ^{35}S production in the Earth's atmosphere. (*B*) Time series of monthly $^{35}SO_4$ concentrations, sunspot number, and rainfall. Error bars stand for ±1 SD of monthly averages. (*C*) Correlations between monthly $^{35}SO_4$ concentrations and sunspot numbers.

($^{35}SO_2$). Nearly all $^{35}SO_2$ is oxidized to radiosulfate ($^{35}SO_4$) aerosol and ultimately deposited on Earth's surface by wet and dry deposition. Compared to the long half-lived ^{10}Be (1.39 million y), which creates a large background in the stratosphere and limits event detection, the shorter half-life of ^{35}S enables more resolved analysis of the solar cycle. Radiosulfur is hitherto overlooked in solar activity studies (2, 3, 8, 9) because of analytical difficulties. Using a newly developed analytical method (11), we present multiyear measurements of atmospheric $^{35}SO_4$ in submicrometer aerosols collected from Southern California to show its response to the most recent solar cycle (*Materials and Methods*).

Results and Discussion

The averaged concentration of $^{35}SO_4$ during 2014 to 2016, the maximum of Solar Cycle 24, is 201 ± 88 molecules·m^{-3} (±1 SD; $n = 102$), significantly lower than our previous measurements made at the same place during the solar minimum at 2009 to 2010 (455 ± 157 molecules·m^{-3}) (12) (Fig. 1*B* and *SI Appendix*). The budget of atmospheric $^{35}SO_4$ is controlled by sources and sinks. Significant differences in rainfall ($^{35}SO_4$ sinks via washout effects) between 2014 to 2016 and 2009 to 2010 are not observed (Fig. 1*B*). Sunspot number indicates the strength of disturbances in the Sun's magnetic field and is conventionally used as an index of solar activity (2). A clear inverse relationship ($P < 0.01$) between monthly sunspot number and $^{35}SO_4$ concentrations is found (Fig. 1 *B* and *C*), consistent with a solar modulation effect in the atmospheric production of cosmogenic radionuclides (2, 8). During solar maximum, GCRs are modulated by the strong solar and geomagnetic fields relative to solar minimum (i.e., shielded by the solar wind as shown in Fig. 1*A*), leading to lower production rates of cosmogenic radionuclides including ^{35}S.

Globally, production rates of ^7Be, ^{10}Be, ^{14}C, ^{22}Na, and ^{36}Cl during solar maximum are ca. 50 to 60% of those during solar minimum (8). The ^{35}S production rate was first estimated to be ∼0.8 of ^{36}Cl by Lal and Peters (10), but it has not been updated for >50 y and its relationship with solar activity has not been studied. Sensitivity tests of a ^{35}S box model with ^{35}S production, transport, transformation, and deposition rates (12, 13) show that a change of ^{35}S production rate by 50% leads to 50% variation in $^{35}SO_4$ concentrations at Earth's surface. Based on the observed ratio of $^{35}SO_4$ at solar maximum to minimum (∼44%), we expect a ^{35}S production rate variation across a 11-y solar cycle to be similar. More rigorous determinations of ^{35}S production yield functions and cross-sections are needed in the future to refine our preliminary estimation. There remains inconstancy in modeling radionuclide production rates by using different yield functions and cross-sections (2, 8, 9). The uncertainty may be propagated to ∼50% at the high-energy ranges of SPEs (9). A reliable cosmogenic radionuclide production model must reproduce measurements of all nuclides including ^{35}S, which is lacking at present.

In reconciling models and observations, proper modeling of radionuclide transport in the turbulent atmosphere with climatic variability is required (2, 6, 9). We note that a sample with extremely high $^{35}SO_4$ concentration (7,390 molecules·m^{-3} during 3 to 7 May 2014) is not included in this study. Our previous detailed analysis (13) showed that the unusual enrichment of $^{35}SO_4$ in this episode is due to an extremely rare deep stratospheric intrusion event. If this sample is included, the average of $^{35}SO_4$ concentrations becomes 271 molecules·m^{-3} and a large SD (714 molecules·m^{-3}) is obtained. The dramatic change of $^{35}SO_4$ at a weather timescale highlights the high sensitivity of ^{35}S to the atmospheric circulation variability because its half-life being on the timescale of atmospheric mixing and conversion to an aerosol offers a more precise definition

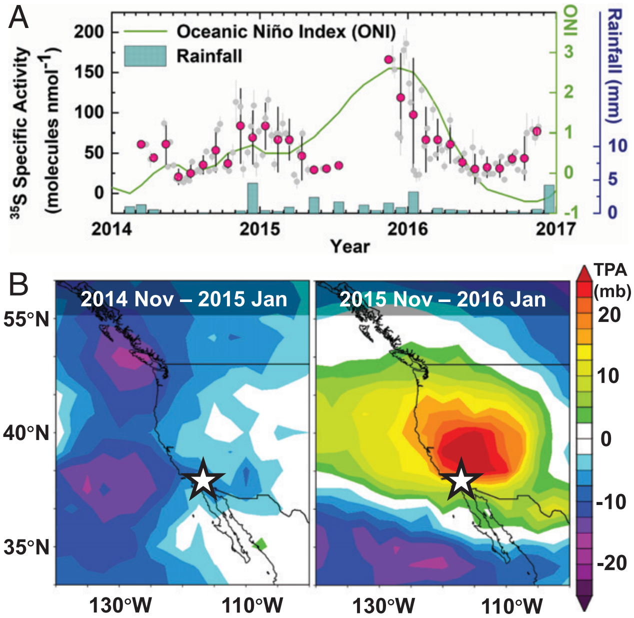

Fig. 2. (*A*) Same as Fig. 1*B* but for monthly ^{35}S-specific activity (see main text and *SI Appendix* for reasoning) and Oceanic Niño Index. The ^{35}S-specific activities in all samples (gray circles; n = 102) are shown with analytical errors. (*B*) Tropopause pressure anomalies (TPA) over the West Coast of the United States (with respect to 1991 to 2020 baselines) in November to January during 2014 to 2015 (*Left*) and 2015 to 2016 (*Right*) calculated from daily National Centers for Environmental Prediction (NCEP) reanalysis data (https://psl.noaa.gov/data/histdata/). The white star indicates our sampling site.

of weather and potentially climate events. To understand climate-induced variability in cosmogenic radionuclides, the 2015/2016 El Niño occurring in our study period serves as an additional case study (*SI Appendix*). It is the longest and strongest among several extreme El Niño events during the "Anthropocene" (e.g., 1982/1983, 1997/1998, 2015/2016), which significantly influenced global climate, society, and economics (14, 15). For example, the anomalous atmospheric circulation during the 1997/1998 El Niño severely disrupted global weather and climate patterns and led to unusual floods and droughts, ultimately resulting in >20,000 fatalities and >35 billion US dollar economic losses worldwide (14). Stratosphere-to-troposphere transport (STT) at midlatitudes became stronger during El Niño events and ultimately altered tropospheric ozone budgets (15).

A clear $^{35}SO_4$ trend during 2014 to 2016 is not found (Fig. 1*B*), suggesting that overall influences of El Niño on absolute $^{35}SO_4$ concentrations are small. There is a distinct rainfall seasonal cycle in our study region (Figs. 1*B* and 2*A*). To correct for washout-induced seasonal changes in $^{35}SO_4$ sinks, required for investigating subtle weekly variability in sources of surface $^{35}SO_4$, we calculate ^{35}S-specific activity (the ratio of $^{35}SO_4$ to stable sulfate concentrations). A distinct seasonal cycle in ^{35}S-specific activity is observed, with peaks in the Santa Ana wind season (fall to spring) (Fig. 2*A*). Santa Ana winds are a special weather feature in Southern California, characterized by strong gusty winds descending from inland deserts to the coast. It is found that ^{35}S-specific activities during November to January at 2015 to 2016 (the peak of 2015/2016 El Niño) are generally higher than in the same season at 2014 to 2015, when the El Niño event was not developed (Fig. 2*A*). The most plausible explanation for this observation is the enhanced input of ^{35}S from the stratosphere to surface via STT events (12). This is supported by climatological analysis showing positive anomalies of tropopause pressures over the West Coast of United States during the peak of 2015/2016 El Niño (i.e., a lower tropopause facilitating STT) (Fig. 2*B*). The ~60% increases in ^{35}S-specific activity during November to January at 2015 to 2016 relative to 2014 to 2015 are significantly higher than early estimations of enhanced STT at midlatitudes induced by El Niño (~25%) (15), probably due to additional coupling of STT with Santa Ana winds (13, 16). Some climatology studies reveal stronger Santa Ana winds during El Niño than La Niña events although others have suggested an inverse relationship (17). Our observations support the former interpretation and highlight the potential role of El Niño in the coupling between STT and Santa Ana winds with societal impacts such as wildfire and air quality (13, 16). Predictions of such climate-induced influences and their potential linkages with solar activities in the future (*SI Appendix*) are an important topic for further investigation (15, 17).

Collectively, this study provides a multiyear investigation on the response of cosmogenic ^{35}S production to 11-y solar cycles. Analysis of weekly ^{35}S variation in extreme El Niño events also resolves climate effects on cosmogenic radionuclide transport and deposition. Although ^{35}S cannot be used in paleoclimate studies due to its short half-life, ^{35}S measurements provide an opportunity to reduce uncertainties within existing cosmogenic radionuclide production and transport models for reconstructions of past astronomical, climatic, and geomagnetic events (2). The advantage of ^{35}S compared to other aerosol-bound radionuclides is the better definition of sulfur chemistry and transport in atmospheric chemistry transport models, although ^{35}S production cross-sections and spallation yields are less studied. A close intercommunity collaboration between atmosphere scientists and nuclear chemists is needed in the future.

Materials and Methods

Submicrometer aerosol samples (<1 μm) were collected weekly at La Jolla (32.7°N, 117.2°W) from March 2014 to November 2016. Radiosulfur was determined by an ultralow-level scintillation counting method designed for aerosol measurements (11). See *SI Appendix* for the full details of analytical methods and data analysis strategies.

Data Availability. The ^{35}S, sunspot (Royal Observatory of Belgium, Brussel), ONI (National Oceanic and Atmospheric Administration Oceanic Niño Index), and rainfall (National Oceanic and Atmospheric Administration Online Weather Data) data have been deposited in Mendeley Data (https://data.mendeley.com/datasets/5wz2xwsc9s).

ACKNOWLEDGMENTS. Conceptualization, data compilation/analysis/interpretation, and manuscript writing conducted at Guangzhou Institute of Geochemistry, Chinese Academy of Sciences (GIGCAS) were funded by the National Natural Science Foundation of China (Grant: 42021002), the Key Research Program of Frontier Sciences from the Chinese Academy of Sciences (Grant: ZDBS-LY-DQC035), the Key Special Project for Introduced Talents Team of Southern Marine Science and Engineering Guangdong Laboratory (Guangzhou) (Grant: GML2019ZD0308), and the Guangdong Pearl River Talents Program (Award: 2019QN01L150) (to M.L.). Laboratory works were carried out at University of California San Diego. We thank Terri Jackson and Rick Thomas for helping in sampler setups and Jon Sigurdson, Erin Hunt, Laura Lu, Xiaolin Zhang, and Xiemin Huang for assistance in collecting a part of the samples. This is contribution no. IS-3169 from GIGCAS.

1. F. Adolphi *et al.*, Persistent link between solar activity and Greenland climate during the Last Glacial Maximum. *Nat. Geosci.* **7**, 662–666 (2014).
2. T. J. Heaton *et al.*, Radiocarbon: A key tracer for studying Earth's dynamo, climate system, carbon cycle, and Sun. *Science* **374**, eabd7096 (2021).

3. I. G. Usoskin, G. A. Kovaltsov, Mind the gap: New precise 14C data indicate the nature of extreme solar particle events. *Geophys. Res. Lett.* **48**, e2021GL094848 (2021).
4. F. Miyake, K. Nagaya, K. Masuda, T. Nakamura, A signature of cosmic-ray increase in AD 774–775 from tree rings in Japan. *Nature* **486**, 240–242 (2012).
5. A. J. Timothy Jull *et al.*, Rapid ^{14}C excursion at 3372-3371 BCE not observed at two different locations. *Nat. Commun.* **12**, 712 (2021).
6. U. Heikkila, J. Beer, J. Feichter, Meridional transport and deposition of atmospheric Be-10. *Atmos. Chem. Phys.* **9**, 515–527 (2009).
7. B. D. Fields *et al.*, Supernova triggers for end-Devonian extinctions. *Proc. Natl. Acad. Sci. U.S.A.* **117**, 21008–21010 (2020).
8. S. V. Poluianov, G. A. Kovaltsov, A. L. Mishev, I. G. Usoskin, Production of cosmogenic isotopes 7Be, 10Be, 14C, 22Na, and 36Cl in the atmosphere: Altitudinal profiles of yield functions. *J. Geophys. Res. Atmos.* **121**, 8125–8136 (2016).
9. F. Mekhaldi, F. Adolphi, K. Herbst, R. Muscheler, The signal of solar storms embedded in cosmogenic radionuclides: Detectability and uncertainties. *J. Geophys. Res. Space Phys.* **126**, e2021JA029351 (2021).
10. D. Lal, B. Peters, "Cosmic ray produced radioactivity on the earth" in *Kosmische Strahlung II/Cosmic Rays II*, K. Sitte, Ed. (Springer, 1967), pp. 551–612.
11. M. Lin, M. H. Thiemens, Accurate quantification of radiosulfur in chemically complex atmospheric samples. *Anal. Chem.* **90**, 2884–2890 (2018).
12. A. Priyadarshi, J. Hill-Falkenthal, E. Coupal, G. Dominguez, M. H. Thiemens, Measurements of S-35 in the marine boundary layer at La Jolla, California: A new technique for tracing air mass mixing during Santa Ana events. *J. Geophys. Res. Atmos.* **117**, D08301 (2012).
13. M. Lin, L. Su, R. Shaheen, J. C. H. Fung, M. H. Thiemens, Detection of deep stratospheric intrusions by cosmogenic 35S. *Proc. Natl. Acad. Sci. U.S.A.* **113**, 11131–11136 (2016).
14. W. J. Cai *et al.*, Increasing frequency of extreme El Nino events due to greenhouse warming. *Nat. Clim. Chang.* **4**, 111–116 (2014).
15. J. L. Neu *et al.*, Tropospheric ozone variations governed by changes in stratospheric circulation. *Nat. Geosci.* **7**, 340–344 (2014).
16. A. O. Langford, R. B. Pierce, P. J. Schultz, Stratospheric intrusions, the Santa Ana winds, and wildland fires in Southern California. *Geophys. Res. Lett.* **42**, 6091–6097 (2015).
17. J. Guzman-Morales, A. Gershunov, J. Theiss, H. Li, D. Cayan, Santa Ana Winds of Southern California: Their climatology, extremes, and behavior spanning six and a half decades. *Geophys. Res. Lett.* **43**, 2827–2834 (2016).